Time-resolved diffuse optical spectroscopy of small tissue samples

Paola Taroni, Daniela Comelli, Andrea Farina, and Antonio Pifferi

ULTRAS-CNR-INFM and IFN-CNR, Politecnico di Milano, Dipartimento di Fisica, Piazza Leonardo da Vinci 32, I-20133 Milano, Italy
paola.taroni@fisi.polimi.it

Alwin Kienle

Institut für Lasertechnologien in der Medizin und Meßtechnik, Helmholtzstr.12, D-89081 Ulm, Germany
alwin.kienle@ilm.uni-ulm.de

Abstract: Time-resolved transmittance spectroscopy was performed in the wavelength range of 610 or 700 to 1050 nm on phantom parallelepipeds and bone tissue cubes of different sizes. The data were best fitted with solutions of the diffusion equation for a laterally infinite slab and for a parallelepiped to investigate how size and optical properties of the samples affect the results obtained with the two models. Monte Carlo simulations were also performed to support and help with the interpretation of the experimental data. The parallelepiped model performs much better than the infinite slab model for the estimate of the reduced scattering coefficient and, even more, the absorption coefficient. It can profitably be used to quantify the optical properties of biological tissue samples and to derive information such as tissue composition, when small volumes are involved.

OCIS codes: (170.0170) Medical optics and biotechnology; (170.3660) Light propagation in tissues; (170.4580) Optical diagnostics for medicine; (170.5280) Photon migration; (170.6510) Spectroscopy, tissue diagnostics; (290.1990) Diffusion

References and links

1. A. H. Hielscher, A.D. Klose, A. K. Scheel, B. Moa-Anderson1, M. Backhaus, U. Netz, and Jürgen Beuthan, "Sagittal laser optical tomography for imaging of rheumatoid finger joints," Phys. Med. Biol. **49**, 1147-1163 (2004).
2. L. Nicolaides and A. Mandelis, "Novel dental dynamic depth profilometric imaging using simultaneous frequency-domain infrared photothermal radiometry and laser luminescence," J. Biomed. Opt. **5**, 31-39 (2000).
3. H. Ottevaere, M. Tabak, D. Aznar, A. Fernandez Fernandez, S. Van Ierschot, F. Berghmans, and H. Thienpont, "Optical fiber sensors for monitoring stress build-up in dental cements," Proc. of the 16th International Conference on Optical Fiber Sensors OFS16 (2003).
4. M. J. Niedre, G. M. Turner, and V. Ntziachristos, "Time-resolved imaging of optical coefficients through murine chest cavities," J. Biomed. Opt. **11**, 064017 (2006).
5. A. Garofalakis, G. Zacharakis, G. Filippidis, E. Sanidas, D. D. Tsiftsis, E. Stathopoulos, M. Kafousi, J. Ripoll, and T. G. Papazoglou1, "Optical characterization of thin female breast biopsies based on the reduced scattering coefficient," Phys. Med. Biol. **50**, 2583-2596 (2005).
6. B. W. Pogue and M. S. Patterson, "Frequency-domain optical absorption spctroscopy of finite tissue volumes using diffusion theory," Phys. Med. Biol. **39**, 1157-1180 (1994).
7. A. Kienle, "Light diffusion through a turbid papallelepiped," J. Opt. Soc. Am. A **22**, 1883-1888 (2005).
8. A. Torricelli, A. Pifferi, P. Taroni, E. Giambattistelli, and R. Cubeddu "In vivo optical characterization of human tissues from 610 to 1010 nm by time-resolved reflectance spectroscopy," Phys. Med. Biol. **46**, 2227-2237 (2001).
9. R. Cubeddu, A. Pifferi, P. Taroni, A. Torricelli, and G. Valentini, "A solid tissue phantom for photon migration studies," Phys. Med. Biol. **42**, 1971–1979 (1997).
10. M. S. Patterson, B. Chance, and B. C. Wilson, "Time-resolved reflectance and transmittance for the noninvasive measureme nt of tissue optical properties," Appl. Opt. **28**, 2331-2336 (1989).

#79109 - $15.00 USD Received 17 January 2007; revised 27 February 2007; accepted 1 March 2007

11. R. C. Haskell , L. O. Svasaand, T. T. Tsay, T. C. Feng, M. S. McAdams, and B.J. Tromberg, "Boundary conditions for the diffusion equation in radiative transfer," J. Opt. Soc. Am. A **11**, 2727-2741 (1994).
12. K. Furutsu and Y. Yamada, "Diffusion approximation for a dissipative random medium and the applications," Phys. Rev. E **50**, 3634–3640 (1994).
13. R. Cubeddu, A. Pifferi, P. Taroni, A. Torricelli, and G. Valentini, "Experimental test of theoretical models for time-resolved reflectance," Med Phys. **23**, 1625-1633 (1996).
14. A. Pifferi, A. Torricelli, A. Bassi, P. Taroni, R. Cubeddu, H. Wabnitz, D. Grosenick, M. Moller, R. Macdonald, J. Swartling, T. Svensson, S. Andersson-Engels, R. L. van Veen, H. J. Sterenborg, J. M. Tualle, H. L. Nghiem, S. Avrillier, M. Whelan, and H. Stamm, "Performance assessment of photon migration instruments: the MEDPHOT protocol, " Appl. Opt. **44**, 2104-2114 (2005).
15. R. L. P. van Veen, H. J. C. M. Sterenborg, A. Pifferi, A. Torricelli, E. Chikoidze, and R. Cubeddu, "Determination of visible near-IR absorption coefficients of mammalian fat using time- and spatially resolved diffuse reflectance and transmission spectroscopy," J. Biomed. Opt. **10**, 054004 (2005).
16. S. Prahl, Oregon Medical Laser Center website: http://omlc.ogi.edu/spectra/water/ index.html.
17. P. Taroni, D. Comelli, A. Pifferi, A. Torricelli, and R. Cubeddu, "Absorption of collagen: effects on the estimate of breast composition and related diagnostic implications," J. Biomed. Opt. **12**, in press.
18. L. S. Lasdon, A. D. Waren, A. Jain, and M. Ratner , "Design and testing of a generalized reduced gradient code for nonlinear programming," ACM Trans. Math. Software **4**, 34-50 (1978).
19. L.-H. Wang, S. L. Jacques, and L. Zheng, "MCML-Monte Carlo modeling of light transport in multi-layered tissues," Computer Methods and Programs in Biomedicine **47**, 131-146 (1995).
20. T. J. Pfefer, J.K. Barton, E. K. Chan, M. G. Ducros, B. S. Sorg, T. E. Milner, J. S. Nelson, and A. J. Welch, "A three-dimensional modular adaptable grid numerical model for light propagation during laser irradiation of skin tissue," IEEE J. Sel. Top. Quantum Electron. **2**, 934-942 (1996).
21. A. Kienle and M. S. Patterson, "Determination of the optical properties of turbid media from a single Monte Carlo simulation," Phys. Med. Biol. **41**, 2221-2227 (1996).
22. F. Martelli and G. Zaccanti, "Calibration of scattering and absorption properties of a liquid diffusive medium at NIR wavelengths. CW method," Opt. Express **15**, 486-500 (2007).
23. A. Pifferi, A. Torricelli, P. Taroni, A. Bassi, E. Chikoidze, E. Giambattistelli, and R. Cubeddu "Optical biopsy of bone tissue: a step toward the diagnosis of bone pathologies," J. Biomed. Opt. **9**, 474–480 (2004).
24. A. Sviridov, V. Chernomordik, M. Hassan, A. Russo, A. Eidsath, P. Smith, and A. H. Gandjbakhche, "Intensity
profiles of linearly polarized light backscattered from skin and tissue-like phantoms," J. Biomed. Opt. **10**, 014012 (2005).
25. A. Kienle, C. Wetzel, A. Bassi, D. Comelli, P. Taroni, and A. Pifferi, "Determination of the optical properties of anisotropic biological media using an isotropic model," J. Biomed. Opt. **12**, in press.
26. D. L. Batchelar, M. T. M. Davidson, W. Dabrowski, and I. A. Cunnigham, "Bone-composition imaging using coherent-scatter computed tomography: Assessing bone health beyond bone mineral density," Med. Phys. **33**, 904-915 (2006).

1. Introduction

Optical techniques are appealing as diagnostic means in medicine, as they are non-invasive, relatively low cost, and can provide functional information. In most cases diagnosis relies on the different optical properties of pathologic versus healthy tissue or on physiologic information that can be derived from the assessment of the optical properties, such as blood oxygenation estimated when the absorption coefficient is known at selected wavelengths.

Light is also used for therapeutic applications, from photoablation of both soft and hard tissues to the photodynamic therapy of tumors and other non-neoplastic lesions. Knowledge about the penetration depth and, more in general, about light distribution in tissues would make the development of optimized protocols feasible, and improve the expected outcomes.

In principle time-resolved measurements, performed either in reflectance or in transmittance geometry, allow the simultaneous assessment of both the absorption and reduced scattering coefficients of turbid media, such as most biological tissues. To this end, experimental data need to be interpreted with a suitable model of light propagation. Most often, a very simple approach is followed, which relies on the diffusion approximation of the radiative transport theory. Simple and fast analytical solutions for homogeneous infinite or semi-infinite media are generally chosen for data analysis. Some experimental situations are well described by that geometry. However, conditions of practical interest exist where the small size of the probed volume cannot be neglected. This occurs *in vivo*, when small parts of the human body are investigated (*e.g.* fingers for the diagnosis of rheumatoid arthritis [1] or

#79109 - $15.00 USD Received 17 January 2007; revised 27 February 2007; accepted 1 March 2007

teeth in dental applications [2,3]), when localized pathologic lesions need to be imaged, or when studies are performed on small animals [4]. Moreover, the small sample size can be an issue also in *ex vivo* applications (*e.g.* analysis of bioptic samples [5]).

The effects of applying a theoretical model that holds for an infinite o semi-infinite medium to a small sample, and their impact on biomedical applications have already been topic of investigation in the past (see *e.g.* [6]). One of the authors (AK) has previously derived a solution of the diffusion approximation that holds for a turbid parallelepiped [7]. Based on comparisons with Monte Carlo simulations, in the diffusive regime the results achieved were good, with the further advantage of a fast convergence of the solution.

In the present work, time-resolved spectral transmittance measurements were performed on phantoms and *ex vivo* on bone samples. For both sample types, parallelepipeds of different sizes were measured, and data were interpreted using the standard solution of the diffusion equation for an infinite slab and the solution for a parallelepiped [7]. The resulting absorption and reduced scattering spectra were compared to illustrate the improvement in measurement accuracy that can be obtained with the latter method. To support the interpretation of the results and contribute to it, Monte Carlo simulations were also performed and fitted with both models of light propagation. In addition, bone tissue composition was derived from the estimated absorption spectra.

2. Materials and methods

2.1 System set-up

The system for time-resolved transmittance spectroscopy (TRS) is described in detail elsewhere [8]. It is fully automated and allows spectroscopic measurements to be performed in the range of 610 to 1050 nm, exploiting a synchronously pumped dye laser (below 700 nm) and an actively mode-locked picosecond Ti:sapphire laser (above 700 nm). For the measurements, 1 mm-plastic-glass fibers (AFS1000, Fiberguide, New Jersey) delivered light to the samples and collected the transmitted photons. A double-microchannel-plate photomultiplier tube (R1564U with S1 photocathode, Hamamatsu Photonics K.K., Japan) and a PC card for time-correlated single-photon counting (SPC-130, Becker and Hickl GmbH, Germany) allowed the assessment of time-resolved transmittance curves every 5 nm from 610 to 1050 nm. A small fraction of the incident beam was coupled to a 1 mm-fiber and fed directly to the photomultiplier tube for on-line recording of the instrument response function (IRF). Overall, the full width at half maximum (FWHM) of the IRF was smaller than 100-120 ps at any wavelength.

A PC controlled the laser tuning and power, and optimized the IRF by automatically adjusting the Lyot filter and the cavity length of the Ti:sapphire laser. To handle a large dynamic range, the detected intensity was adjusted with a variable neutral density filter mounted on a stepper motor and placed in the illumination path. The total number of collected photons per second was used as input in a feedback loop, aiming at a signal of about 400,000 counts/s. At any wavelengths, 4 subsequent measurements were performed, each with an acquisition time of 1 s.

2.2 Phantoms

TRS measurements were carried out from 700 to 1050 nm on four homogeneous phantoms shaped as rectangular parallelepipeds with different base size (1 x 1 cm^2, 2 x 2 cm^2, 3 x 3 cm^2 and 5 x 5 cm^2), but all with the same thickness (2 cm). All phantoms were made of the same aqueous solution of 1.8% Intralipid, with 2% agar added to obtain a solid slab, as described in detail in Ref. 9. The injection and collection fibers were placed centered and orthogonal to the top and bottom surfaces, respectively, and in contact with them.

2.3 Ex vivo *bone samples*

A porcine head was purchased from the slaughter. The skull was excavated and three cubical blocks were cut from the skull using an inside hole saw within a few hours. Then, the samples

#79109 - $15.00 USD Received 17 January 2007; revised 27 February 2007; accepted 1 March 2007

were ground manually (mesh 400/600) to obtain cubes with side lengths of 1.1, 1.5, and 1.6 cm.

The cubes were stored in an isotonic NaCl-solution until the measurements were performed. The injection and collection fibers were placed centered, orthogonal to and in contact with two opposite sides. TRS measurements were performed along three orthogonal directions. On the smallest sample (1.1 cm-side), for a technical problem, measurements were carried out only along two directions. On one sample (1.5 cm-side), measurements were performed over an extended spectral range (610-1050 nm). On other samples, measurements were carried out from 700-1050 nm.

2.4 Data analysis

The absorption and reduced scattering coefficients (μ_a and μ'_s, respectively) were estimated by fitting the experimental data to an analytical solution of the diffusion approximation of the transport equation for: i) a homogeneous infinite slab [10], and ii) a homogeneous parallelepiped [7].

With both models, the extrapolated boundary condition [11] was used, and the diffusion coefficient D was assumed to be independent of the absorption properties of the medium (*i.e.* $D = 1/(3\mu'_s)$) [12]. The refractive index was fixed at 1.33 for phantoms, 1.40 for bone tissue, and 1.00 for the external medium (*i.e.* air).

As shown in details in Cubeddu *et al* [13], the theoretical time-dispersion curve was convolved with the IRF and normalized to the area of the experimental curve. The fitting range included all points with a number of counts higher than 80% of the peak value on the rising edge of the curve and 1% on the tail. The best fit was reached with a Levenberg-Marquardt algorithm by varying both μ'_s and μ_a to minimize the error norm χ^2.

The 4 measurements performed at each wavelength were best fitted separately, and the results were then averaged.

The reproducibility in the estimate of the optical coefficients was calculated by repeating measurements of the same phantom under the same experimental conditions in 4 different days. The results produced a coefficient of variation of 5.6% for μ_a and 6.5% for μ'_s [14].

To estimate bone tissue composition, based on the Beer's law the absorption spectra were best fitted to reference spectra of lipids [15], water, oxy- (oxyHb) and deoxy-hemoglobin (deoxyHb) [16], and collagen [17], as a main absorber of the hard bone matrix. The effect of a free wavelength-independent background was also tested. The best fit was reached with a generalized reduced gradient non-linear optimization algorithm [18] by varying the concentrations of the sample constituents (and, in case, of the wavelength-independent background) to minimize the error sum between experimental and theoretical sample absorption. A commercial tool was used for this purpose (Microsoft Excel Solver).

2.5 Monte Carlo simulations

In order to investigate the errors due to the approximations of the diffusion theory, we fitted its solutions for an infinite slab and for a rectangular parallelepiped to the time-resolved transmittance from a rectangular parallelepiped simulated with the Monte Carlo method. The same sizes as for the phantoms were considered.

The principles of the Monte Carlo method to describe light propagation in turbid media can be found in the literature [19]. In our simulations the parallelepiped was illuminated perpendicular onto the middle of one of the bases and the time-resolved transmittance from the middle of the opposite base was stored. We assumed a refractive index of 1.33 inside and of 1.00 outside the parallelepiped representing our phantom samples and air, respectively. When a photon propagated to one of the parallelepiped borders the probability for reflection and transmittance was calculated using Fresnel reflection [20]. The simulations were performed for a reduced scattering coefficient of 15 cm^{-1} and an absorption coefficient of 0 cm^{-1}. The time-resolved transmittance for finite absorption coefficients was obtained by scaling the data for $\mu_a = 0$ cm^{-1} with the Lambert-Beer law [21] for two reasons. First, it

#79109 - $15.00 USD Received 17 January 2007; revised 27 February 2007; accepted 1 March 2007

allows one to calculate the time-resolved transmittance data for a series of absorption coefficients from one simulation. Second, it accelerates the calculation time even for a single simulation, because the probability for transmittance is increased using μ_a = 0 cm^{-1}. A Henyey-Greenstein function with an anisotropy factor of 0.8 was used as phase function.

Single-wavelength time-resolved simulated curves were then fitted with both the infinite slab and parallelepiped models, following the same procedure as used for phantom and bone data (Section 2.4).

3. Results and discussion

3.1 Phantom measurements

To investigate the effects of the limited size of parallelepiped samples on the interpretation of time-resolved transmittance data with the solution of the diffusion equation for an infinite slab, measurements were performed on parallelepiped phantoms of equal composition and thickness, but different side length. In the phantoms water is by far the primary absorber, if not the only one. Taking its absorption properties into account, spectral measurements were performed between 700 and 1050 nm. This allowed us to investigate continuously the behavior in the entire interval of μ_a = 0-0.5 cm^{-1}, that is in the range of main interest for biological tissues. Similarly, μ'_s is expected to change between about 10 and 20 cm^{-1} with wavelength.

Figure 1 reports the corresponding absorption and reduced scattering spectra. The absorption spectrum of water [16] is also displayed in Fig. 1(a), as a reference of the expected absorption spectra of the phantoms [22]. Only for the widest sample (5 cm-side), the absorption properties could be assessed with good accuracy over the entire wavelength range. For all other phantoms, significant discrepancy was observed, leading to estimated μ_a values that are always higher than expected. It is worth noting that the smaller the sample size the bigger the error, with a strong worsening for the smallest sample. For measurements performed on the same phantom, at wavelengths where the absorption is weaker, the absolute error is slightly more marked. The combination of these two effects (e.g. small size and low absorption) can lead to exceedingly high values of the estimated absorption. Specifically, for the smallest sample at short wavelengths (λ < 830 nm) the fitted μ_a is about 0.28-0.30 cm^{-1}, that is about 10 times higher than the water absorption.

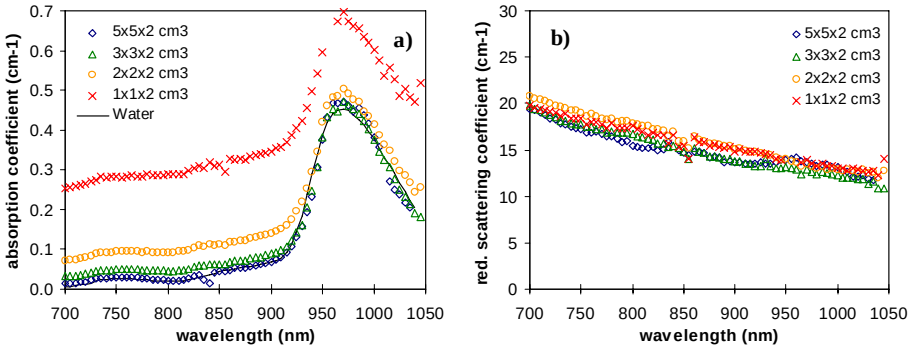

Fig 1. Absorption (a) and reduced scattering (b) spectra of parallelepiped phantoms of different sizes as obtained with the infinite slab model. As a reference, the absorption spectrum of water is also reported. Median standard deviations for 4 repeated measurements of the absorption spectra were: ◊, 0.0010 cm^{-1}; Δ, 0.0010 cm^{-1}; ○, 0.0013 cm^{-1}; ×, 0.0031 cm^{-1}. Median standard deviations for 4 repeated measurements of the reduced scattering spectra were: ◊, 0.13 cm^{-1}; Δ, 0.10 cm^{-1}; ○, 0.11 cm^{-1}; ×, 0.13 cm^{-1}.

#79109 - $15.00 USD Received 17 January 2007; revised 27 February 2007; accepted 1 March 2007

For what concerns the estimated scattering properties (Fig. 1(b)), smaller samples seem to lead to slightly higher values of the estimated μ'_s, and the difference seems little more marked at short wavelengths. However, the dependence on the sample size is much smaller than observed for the absorption properties and, taking into account the noise of the measurement and of the fitting procedure, it is much less obvious to identify the effects of sample size and optical properties.

The results obtained from fitting the phantom data with the solution of the diffusion equation for a parallelepiped are shown in Fig. 2. All fitted absorption spectra closely resemble the absorption of water (Fig. 2(a)), except for the one obtained for the smallest phantom. In that case, high absorption values are slightly underestimated. However the error is always smaller than 10%. As compared to the water absorption, some overestimate is observed at short wavelengths, where the absorption is weak. However, the difference is of about 0.015 cm^{-1} or smaller, and it could at least in part be due to the absorption of phantom components other than water.

All reduced scattering spectra (Fig. 2(b)) overlap, suggesting that the model can account for the limited size of the samples. Only the spectrum of the widest parallelepiped differs from the others at short wavelengths (λ < 800 nm) and on the absorption peak of water (950-1000 nm), where it seems to be affected by some cross-coupling between the estimated scattering and the absorption properties. The two models yield slightly different μ'_s values, lower for the parallelepiped model, with differences that can reach 10% for the smallest sample.

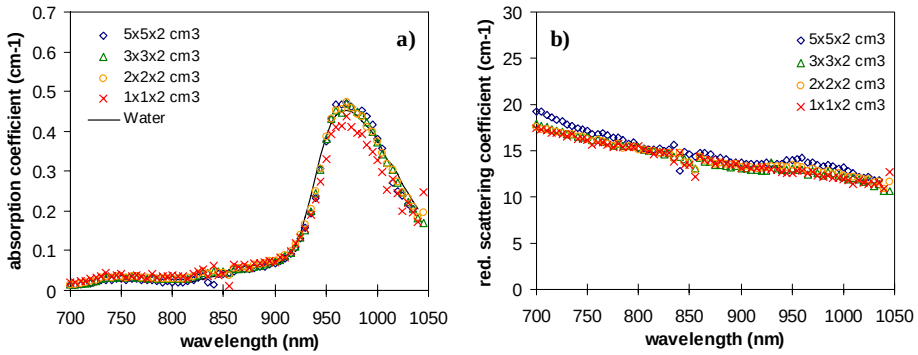

Fig. 2. Absorption (a) and reduced scattering (b) spectra of parallelepiped phantoms of different sizes as obtained with the parallelepiped model. As a reference, the absorption spectrum of water is also reported. Median standard deviations for 4 repeated measurements of the absorption spectra were: ◊, 0.0010 cm^{-1}; Δ, 0.0012 cm^{-1}; ○, 0.0019 cm^{-1}; ×, 0.0048 cm^{-1}. Median standard deviations for 4 repeated measurements of the reduced scattering spectra were: ◊, 0.12 cm^{-1}; Δ, 0.11 cm^{-1}; ○, 0.11 cm^{-1}; ×, 0.13 cm^{-1}.

3.2 Monte Carlo simulations

To support the observations on phantom results, Monte Carlo simulations were performed, convolved with the IRF and best fitted with either of the two models, using the same procedure as for the experimental data. The reduced scattering was fixed (μ'_s = 15 cm^{-1}), while the absorption coefficient was varied in the range of μ_a = 0-0.5 cm^{-1}. Those values were chosen as representative of the typical optical properties of biological tissues at near-infrared wavelengths, and thus they correspond to the properties of the phantoms that were selected with the same purpose. The same sample sizes as for the phantoms were also chosen.

Figure 3(a) shows how the absorption estimates obtained with the infinite slab model compare with the correct values for various sample sizes. The results are very good for the two wider parallelepipeds. For the smaller ones, a progressive overestimate of the fitted

#79109 - $15.00 USD Received 17 January 2007; revised 27 February 2007; accepted 1 March 2007

absorption is observed. The error increases rapidly upon decreasing the sample size, while it is independent of the absorption value. For the smallest sample, the overestimate is of about 0.28 cm^{-1}, in good agreement with what observed for the phantoms.

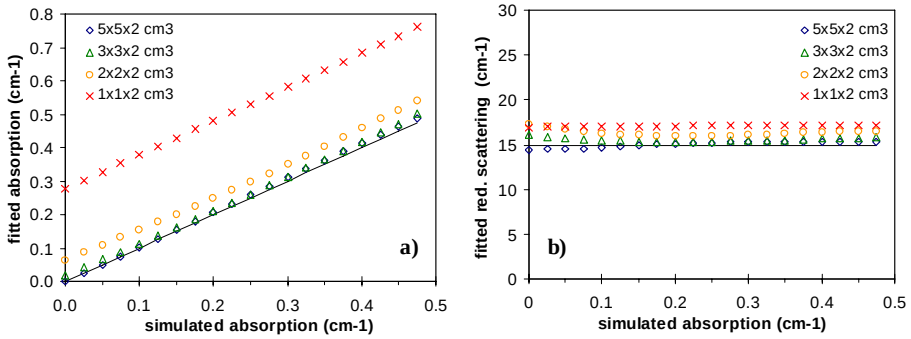

Fig. 3. Absorption (a) and reduced scattering (b) values obtained by best fitting Monte Carlo simulations with the infinite slab model.

The estimated reduced scattering (Fig. 3(b)) depends much less on the sample size, leading at most to an overestimate of ~2 cm^{-1} for the smallest parallelepiped. Some dependence on the absorption properties is detected, but it seems not to be systematic or possibly to come from different contributions.

Absorption values estimated with the parallelepiped model are reported in Fig. 4(a). Essentially, no overestimate independent of the absorption properties is observed, except for a minor contribution that affects the results for the smallest sample. On the other hand, we observed a small overestimate that increases both increasing the absorption value and decreasing the sample size. However, the error is always smaller than 0.066 cm^{-1} (14%) even for the smallest sample with μ_a = 0.475 cm^{-1}.

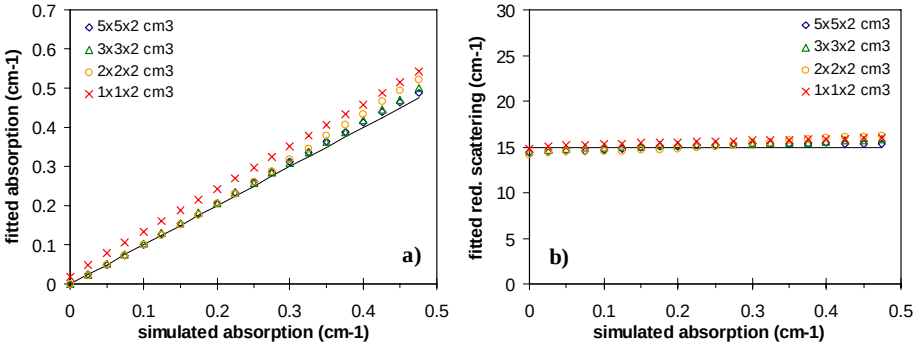

Fig. 4. Absorption (a) and reduced scattering (b) values obtained by best fitting Monte Carlo simulations with the parallelepiped model.

The situation is similar for the reduced scattering properties (Fig. 4(b)). Increasing absorption values lead to a small progressive increase in the estimated μ'_s, suggesting some coupling between the optical coefficients, in agreement with what was observed for phantoms. Still, the fitted μ'_s is always within the range 14-16 cm^{-1}.

Some simulations were performed also with a lower scattering value (μ'_s = 7 cm^{-1}). The situation does not change significantly for what concerns the estimate of the scattering properties. On the other hand, the offset in the estimate of the absorption with the slab model

#79109 - $15.00 USD Received 17 January 2007; revised 27 February 2007; accepted 1 March 2007

increases markedly (approximately by a factor of 2). When the smallest sample is considered, even the parallelepiped model cannot fully compensate for the small sample size, and some offset is observed. However, it is 4-5 times smaller than with the slab model even in the worst case. When the scattering is reduced, photons collected at late times are more sensitive to the sample boundaries than early photons. The information on the scattering and absorption properties is carried mostly by the rising edge and by the tail of the transmittance curve, respectively. This explains why, when a lower scattering is considered, the estimate of the reduced scattering coefficient is less sensitive to the sample boundaries than the estimate of the absorption coefficient.

3.3 Ex vivo *bone measurements: optical properties*

The absorption spectra of bone samples estimated using the infinite slab model are reported in Fig. 5(a). A main peak is observed around 980 nm. A much weaker peak at 760 nm and a shoulder around 930 nm can barely be detected and seem not to be present in the spectra of the smallest sample (1.1 cm-side).

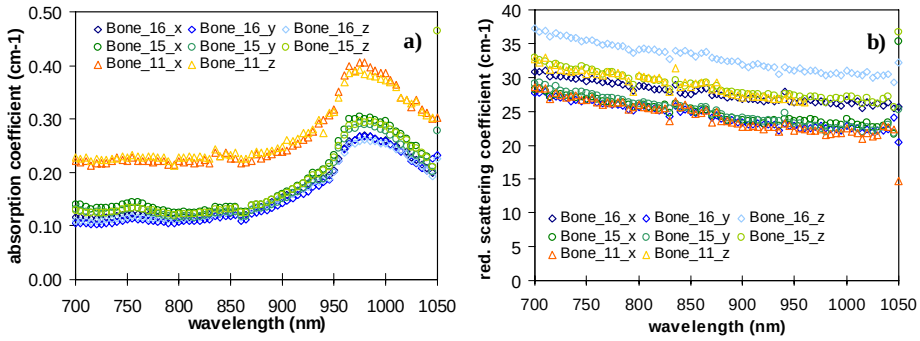

Fig. 5. Absorption (a) and reduced scattering (b) spectra of bone cubes of different sizes as obtained with the infinite slab model. Median standard deviations for 4 repeated measurements of the absorption spectra averaged over the 3 measurement directions were: ◊, 0.0014 cm^{-1}; ○, 0.0016 cm^{-1}; Δ, 0.0032 cm^{-1}. Median standard deviations for 4 repeated measurements of the reduced scattering spectra averaged over the 3 measurement directions were: ◊, 0.21 cm^{-1}; ○, 0.20 cm^{-1}; Δ, 0.24 cm^{-1}.

The absorption spectra measured along orthogonal directions on the same sample are very similar. Smaller sample sizes lead to increased offsets, similar to what was already observed for the phantoms. Specifically, reducing the sample size from 1.5-1.6 cm to 1.1 cm, the offset increases by approximately 0.1 cm^{-1} over the entire spectral range (700-1050 nm), with no clear dependence on the measured absorption. Based on the results of phantom measurements and taken the expected absorption properties of bone [23] into account, an offset is likely to affect also the measurements performed on the two bigger samples.

The reduced scattering spectra (Fig. 5(b)) decrease quite slowly but progressively with wavelength, and show no coupling with the absorption coefficient.

Different from the absorption, the scattering properties depend significantly on the measurement direction, in agreement with the microscopic structure of bone, and in particular with the presence of trabeculae that are expected to make light propagation anisotropic [24]. On the contrary, if the scattering properties averaged over the different measurement directions are considered (data not shown), no main effect of the sample size is observed, with differences smaller than 8% and not systematic with sample size, while differences with measurement direction can be higher than 15%.

The results obtained using the diffusion model for the parallelepiped are shown in Fig. 6. The line shape of the absorption spectrum (Fig. 6(a)) is not significantly different from what obtained with the slab model, but the estimated absorption values are much lower, and the

#79109 - $15.00 USD Received 17 January 2007; revised 27 February 2007; accepted 1 March 2007

difference is more marked for smaller samples. This confirms the hypothesis that an offset affects the absorption coefficient estimated with the slab model, even in the case of the biggest sample. Specifically, by comparison with what obtained with the parallelepiped model, an offset of 0.062 ± 0.008 cm^{-1} can be expected when data for the 1.5 cm-sample are interpreted with the slab model.

We also note that the estimated absorption seems to change slightly with the measurement direction and the changes in absorption correlate positively with the changes observed in the scattering properties (see below and Fig. 6.(b)), even though the former are much smaller. We have previously shown [25] that the absorption estimates obtained interpreting time-resolved reflectance measurements with the diffusion theory for a semi-infinite homogeneous medium are not sensitive to the sample anisotropy. Thus, the correlation observed here could be due to some unexpected physical difference in the sample properties or could be an artifact caused by the heterogeneity of the sample that the model does not account for.

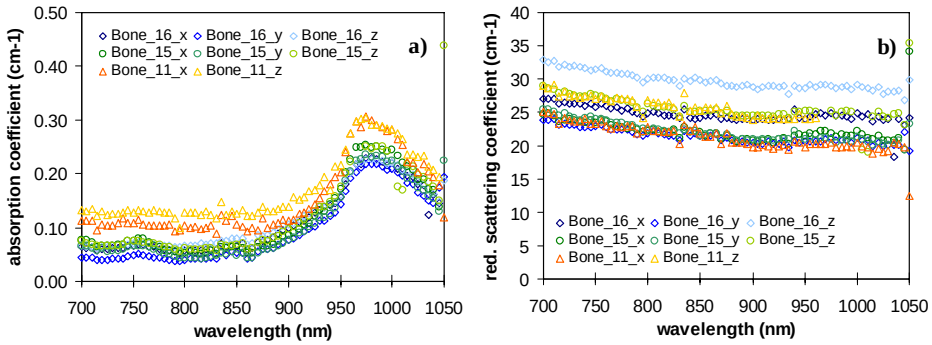

Fig. 6. Absorption (a) and reduced scattering (b) spectra of bone cubes of different sizes as obtained with the parallelepiped model. Median standard deviations for 4 repeated measurements of the absorption spectra averaged over the 3 measurement directions were: ◊, 0.0020 cm^{-1}; ○, 0.0023 cm^{-1}; Δ, 0.0046 cm^{-1}. Median standard deviations for 4 repeated measurements of the reduced scattering spectra averaged over the 3 measurement directions were: ◊, 0.23 cm^{-1}; ○, 0.22 cm^{-1}; Δ, 0.25 cm^{-1}.

The reduced scattering spectra (Fig. 6(b)) are similar to those obtained with the slab model for the marked dependence on the measurement direction and the much smaller effect of the sample size. For what concerns the absolute values of μ'_s, their estimates are typically 10% smaller when the parallelepiped model is used, in good agreement with the results obtained for phantom measurements. As already observed for the phantoms, some coupling between reduced scattering and absorption is present and can be observed around 980 nm (corresponding to the absorption maximum).

3.4 Ex vivo *bone measurements: tissue composition*

The estimate of the optical properties of biological tissues is often performed for diagnostic purposes. In particular, information on tissue composition is derived from the absorption properties.

To understand how the small sample size can affect that process, the Beer's law was applied to interpret the absorption spectra of bone samples obtained with both the slab and the parallelepiped models. Since the presence of sharp features in the absorption spectra makes the fitting procedure more robust, TRS measurements were performed on one bone sample (1.5 cm-side) over an extended spectral range. This allowed us to include a short wavelength region (610-700 nm), where the absorption decreases rapidly with wavelength. The absorption

#79109 - $15.00 USD Received 17 January 2007; revised 27 February 2007; accepted 1 March 2007

spectra obtained performing TRS measurements along three orthogonal directions were averaged, as we did not expect any significant dependence of the absorption properties on the measurement direction.

Contributions from lipids, water, oxyHb, deoxyHb, and collagen were always taken into account. Collagen and hydroxyapatite are the two main components of bone matrix. We have recently measured the absorption spectrum of collagen, while, to our knowledge, no information is available on hydroxyapatite. However, some preliminary measurements suggested that hydroxyapatite is a weak absorber in the red and near-infrared spectral range. So, we decided to consider only collagen.

Based on the results of Monte Carlo simulations and phantom measurements, one of the main effects of the small sample size on the estimate of the absorption properties with the slab model is a significant overestimate, independent of the absorption value. Thus, the effect of a free wavelength-independent background was also tested, to determine whether it could somehow "take care" of the limitations of the slab model for small samples and lead to an acceptable estimate of tissue composition.

Table 1 summarizes the results of the fitting procedure performed testing the effect of the constant background. The concentrations of lipid, water, and collagen were determined based on densities of 0.91, 1.00, and 1.30 g/cm^3, respectively [26]. It should be taken into account that collagen powder can have a significantly different structure as compared to collagen in physiologic conditions, and this can affect its density and, consequently, the assessment of its percentage content in bone tissue.

Table 1. Bone tissue composition, based on different combinations of tissue constituents, as derived from the absorption spectra obtained with the slab and parallelepiped models

	Slab model		**Parallelepiped model**	
Constituents	**Fit #1**	**Fit # 2**	**Fit #1**	**Fit # 2**
Background (cm^{-1})	-	0.085	-	0.000
DeoxyHb (μM)	0.0	4.5	4.0	2.0
OxyHb (μM)	23.5	3.4	3.3	2.3
Lipid (%)	*0.0*	*30.6*	*22.5*	*20.3*
Lipid (mg/cm^3)	0	278	205	185
Water (%)	*31.6*	*38.9*	*41.9*	*41.2*
Water (mg/cm^3)	316	389	419	412
Collagen (%)	*34*	*7*	*15*	*18*
Collagen (mg/cm^3)	446	92	196	236

For the slab model tissue composition estimated without background (Fit #1) is unrealistic, with no lipid and deoxyHb and quite a high oxyHb content. The results of the fit are also very sensitive to the initial values. When the wavelength-independent background is included (Fit #2), its best-fitted value is of 0.085 cm^{-1} and the quality of the fit improves significantly, as judged visually and based on the mean square error MSE that decreases from 1.7 x 10^{-4} cm^{-1} to 1.5 x 10^{-5} cm^{-1}. The contributions of the different constituents seem more realistic, but the results of the fitting procedure still depend clearly on the initial conditions.

When the parallelepiped model is used, the fitting becomes more stable. Even when a free background is considered, its optimal value is zero, suggesting that the model introduces no significant overestimate of the absorption values. Also the MSE value is similar in both cases (2.2 x 10^{-5} cm^{-1} and 1.7 x 10^{-5} cm^{-1} with and without background, respectively). The OxyHb

#79109 - $15.00 USD Received 17 January 2007; revised 27 February 2007; accepted 1 March 2007

and deoxyHb concentrations up to 3 and 4 μM, respectively, are estimated, with lipid and water contents of about 20% and 40%, respectively. It should be taken into account that a water content higher than in physiological conditions is expected, since the samples were kept in an aqueous solution till the measurement time. The estimated concentration of collagen is of about 200-240 mg/cm^3.

4. Conclusions

In conclusion, we have tested a solution of the diffusion theory that holds for a parallelepiped and compared it to the standard solution for an infinite slab. TRS measurements were performed on parallelepiped phantoms of different sizes, with optical properties in the range typical for biological tissues and, in particular, similar to what expected for bone tissue. Monte Carlo simulations were also performed to reproduce the experimental conditions and allow a systematic test of the diffusion models. Finally, TRS data obtained from small bone samples were interpreted, to estimate their optical properties and derive bone tissue composition from the absorption spectra.

For small samples the parallelepiped model performs significantly better than the slab model and allows an accurate assessment of their optical properties (down to sizes of approximately 1.5 cm in the case of bone tissue). The improvement is specially marked for the estimate of the absorption coefficient. Moreover, the solution is characterized by fast convergence that makes it particularly suitable for practical applications. Finally, the fitting procedure for the estimate of tissue composition is definitely more stable and leads to more realistic results when the parallelepiped model is applied.

All these features suggest that it could be profitably used in research studies and diagnostic applications that involve the estimate of the optical properties of small tissue samples.

Acknowledgments

Financial support by the access to research infrastructure activity in the Sixth Framework Programme of the EU contract RII3-CT-2003-506350, Laserlab Europe for conducting the research is gratefully acknowledged.

#79109 - $15.00 USD Received 17 January 2007; revised 27 February 2007; accepted 1 March 2007